Temperature dependence of coherent phonon dephasing in $CsPbCl_3$ nanocrystals

P. Němec and P. Malý
Faculty of Mathematics and Physics, Charles University in Prague, Ke Karlovu 3, 121 16 Prague 2, Czech Republic
(Received 5 August 2005; revised manuscript received 27 October 2005; published 19 December 2005)

We report on the generation of coherent optical phonons in $CsPbCl_3$ nanocrystals in CsCl by femtosecond laser-pulse illumination. Four phonon modes were identified in the measured oscillations of transient transmission with frequencies matching well those of the lowest confined optical-phonon modes in $CsPbCl_3$ nanocrystals. The temperature dependence of the phonon mode softening and oscillation damping was used to identify the phonon dephasing mechanisms. It was shown that the main contribution is due to the effect of cubic anharmonicity of the lattice. The possible role of the spatial confinement of phonons in the volume of nanocrystals and the effects of the nanocrystal size distribution in the oscillation damping are also discussed.

DOI: 10.1103/PhysRevB.72.235324 PACS number(s): 78.67.Bf, 78.47.+p, 42.65.Dr

I. INTRODUCTION

Coherent phonons can be generated in solids by ultrashort laser pulses with pulse duration much shorter than the period of phonon vibration. Generation of coherent phonons by femtosecond laser pulses was demonstrated in various materials, such as semiconductors, semimetals, superconductors, dielectric materials, and molecular crystals.[1,2] The availability of coherent optical phonons at THz frequencies has led to a variety of suggestions for applications and experiments involving, in particular, time-domain spectroscopy of phonons, conversion of mechanical into coherent electromagnetic energy, and proposals on photon control of the ionic motion.[1] In a typical experiment, the generation of coherent phonons by a strong pump pulse results in an oscillation of the transmitted or reflected intensity of the probe beam as a function of the time delay between pump and probe pulses. The oscillations are induced by the modulation of dielectric constant due to the ion motion.[1,2] The decay of coherent phonons can be monitored directly by measuring the damping rate of signal oscillations in the pump and probe reflection or transmission experiments. The present theoretical understanding of the coherent phonon generation is still not certain. Although there is a widespread agreement that stimulated Raman scattering is the key generation mechanism in the transparent region, the generation mechanism in opaque materials is still controversial.[1–4]

Since the early 1980s the properties of low-dimensional semiconductor structures have been extensively studied, particularly those of quantum dots or nanocrystals (NCs).[5] This attention has been motivated both by the fundamental interest in the novel physical properties of such systems and by their potential practical applications in electronic and optoelectronic devices. There has been much interest in the properties of phonons in NCs due to their role in carrier dephasing and relaxation. Optical phonons were investigated mainly by Raman scattering that enabled the elucidation of the role of confinement-, surface-, and disorder-related effects on the phonon frequencies and selection rules.[6–8] The observed low-frequency shift of the peaks in the Raman spectra, accompanied by the line broadening and asymmetry, is usually interpreted in terms of formation of confined phonon modes with frequencies that are redshifted with respect to the corresponding bulk phonon frequency.[8–11] On the other hand, much less is known about the dynamics of *coherent* optical phonons in NCs. Thus far, there appeared only a few reports on coherent optical-phonon generation in semiconductor NCs (NCs of CdSe,[12] $CdTe_{1-x}Se_x$,[13] PbS,[14] and InP[15]) but in none of them the optical-phonon dephasing mechanisms were investigated in detail.

We report on dynamics of four coherent optical-phonon modes in $CsPbCl_3$ nanocrystals in CsCl host matrix. Cesium lead chloride ($CsPbCl_3$) is a rather untypical semiconductor[16,17] whose investigation has been motivated mainly by its possible application as a scintillator or an ionic conductor.[18,19] The Wannier-type excitons (the exciton Bohr radius a_B=0.984 nm) persist up to room temperature (due to the large exciton binding energy of 67 meV) with a fundamental optical transition in a blue spectral region (3.07 eV at 300 K).[16] This makes this material attractive also for photonics and optoelectronics. $CsPbCl_3$ has the perovskite-type structure with a rich phonon spectrum, which was studied both theoretically and experimentally.[19–21] The preparation and properties of $CsPbCl_3$ NCs in CsCl host matrix were described in Ref. 22. The existence of several optical-phonon modes in $CsPbCl_3$ makes the corresponding NCs rather interesting also for the investigation of the properties of spatially confined phonons. Recently, we reported on observation of coherent optical phonons in $CsPbCl_3$ NCs.[23] On basis of the spectral behavior of the initial phase of the mode oscillations, we identified the displacive (impulsive) mechanism of coherent phonon generation in case the material is opaque (transparent) for the incident light. In the current paper we deal with the effect of temperature on the coherent phonon oscillations; that is, we concentrate on the optical-phonon dephasing mechanism in $CsPbCl_3$ NCs.

II. EXPERIMENTAL

The preparation of $CsPbCl_3$ NCs in the CsCl host matrix was described in Ref. 22. The sample studied was obtained by annealing of CsCl:Pb (containing 0.1% of Pb) at 220 °C for 15 h. It contains NCs with volume filling factor of 10^{-6}. The mean size of nanocrystals is about $2R \approx 4$ nm.[22] A rather low-filling factor of NCs in the sample is the reason of the

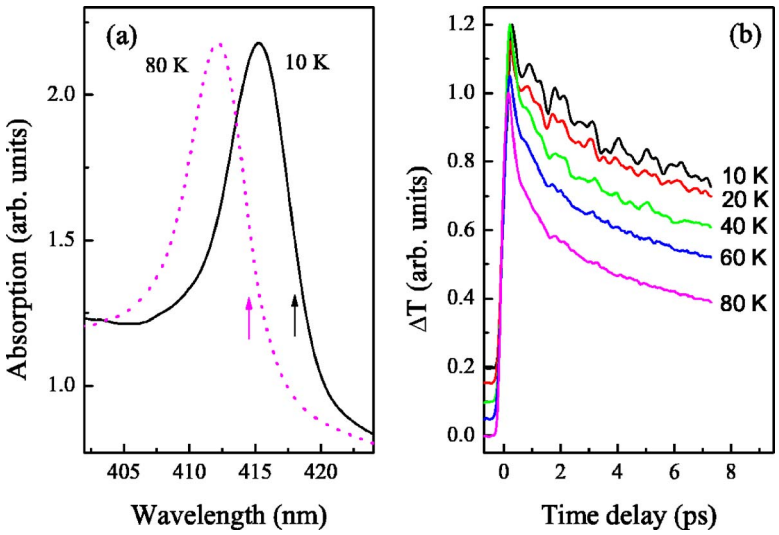

FIG. 1. (Color online) Absorption spectrum of $CsPbCl_3$ nanocrystals in CsCl at 10 and 80 K (a). The arrows represent the central wavelength of the laser pulses used to measure the dynamics of transmission change ΔT shown in (b). The measured traces of ΔT are normalized and vertically shifted for clarity.

failure of the standard TEM analysis of NCs sizes and size distribution. All the reported values of NCs sizes in this material were obtained indirectly.[22,24,25] Our sample was produced in the same way as samples used in Ref. 22, where the NCs size of 4 nm was reported. The size dispersion in our sample can be estimated on the basis of optical measurements.[24,25] In particular, the spectral width of the low-temperature exciton absorption band (cf. Fig. 1(a) and Ref. 26) can be used to determine the inhomogeneous broadening of the optical transition. After deconvolution with the response function of our setup, the measured data imply an upper limit of the inhomogeneous broadening of the linewidth [full width at half maximum (FWHM)] of about 25 meV.[26] The broadening is due to the dispersion in NCs sizes, as the confinement-induced blueshift of the transition energy ΔE depends strongly on the NCs radius R: $\Delta E = \hbar^2\pi^2/(2mR^2)$.[5] In the case of the so-called weak confinement regime ($R \gg a_B$), with the exciton mass $m \approx 2.6m_0$,[27] we obtained the upper limit of 15% in the NCs size distribution. (In fact, the carriers in our NCs are rather in the intermediate confinement regime for which there is no simple formula for calculation of ΔE. The calculation using the strong confinement regime ($R \ll a_B$) approach would lead to an upper limit of 4% in the NCs size distribution.)

The photoexcited carrier dynamics were investigated by the degenerate pump and probe technique. The source of femtosecond pulses ($\tau_p \approx 80$ fs, repetition rate 82 MHz, spectral width FWHM of 15 meV) was the titanium sapphire laser (Spectra-Physics, Tsunami) and β-barium borate (BBO) frequency doubler. The pump and probe beams of the same wavelength with the linear and mutually orthogonal polarizations intersected under the 5° angle in the sample. An optical delay line was used to vary the time delay between pump and probe pulses. The peak intensities in the pump and in the probe pulses were 20 and 1 MW cm^{-2}, respectively. As a measure of transmission changes, we use differential transmission, $\Delta T = T_E - T_0$, where T_E (T_0) is the spectrally integrated transmission of the probe pulse with (without) the pump. The zero time delay was independently determined for each wavelength and temperature by measuring the interference pattern created by pump and probe pulses as a function of their mutual time delay. The measurements were done at temperatures from 10 to 100 K, and the sample was mounted on the cold finger of the closed-cycle helium cryostat (Janis Cryogenics).

III. RESULTS AND DISCUSSION

The investigated sample contains semiconductor NCs with radii slightly larger than the exciton Bohr radius (so-called intermediate confinement regime). Their absorption spectrum is dominated by a strong excitonic absorption, which exhibits an anomalous blueshift with increasing temperature, as illustrated in Fig. 1(a). The results of the degenerate pump and probe experiment at various temperatures are shown in Fig. 1(b), where the change of the probe pulse transmission ΔT is plotted as a function of the time delay between the pump and probe pulses. The laser wavelength of 418 nm at 10 K [marked by an arrow in Fig. 1(a)] was selected at the central position of the spectral interval investigated in Ref. 23. During the measurement of the temperature dependence, the wavelength of the femtosecond laser pulses was tuned to follow the energy shift of the absorption spectrum. The optical creation of excitons leads to an increase in the transmission (absorption bleaching). The decay-time constant of the transient transmission ΔT, which reaches the values from several picoseconds to several tens of picoseconds, depends on the laser wavelength [Fig. 1(b) in Ref. 23] and on the sample temperature [Fig. 1(b)]. We interpret it in terms of the exciton dynamics as will be addressed elsewhere.[28] Here we concentrate on the oscillations observed in the measured signal of ΔT. As can be seen in Fig. 1(b), the oscillations are rather complex and their damping rate increases with increasing temperature.

In order to extract the oscillations, we have numerically computed the time derivative of the measured signal of ΔT and subtracted a monotonously decreasing function from the data. The procedure of the analysis of data was described previously in Ref. 23. Numerical Fourier analysis of the oscillations reveals that they are, in fact, formed by four distinct oscillation modes [see inset of Fig. 1(b) in Ref. 23]. For example, at a temperature of 10 K we found the following

TABLE I. Parameters of bulk $CsPbCl_3$ and values of constants for $CsPbCl_3$ NCs obtained from the analysis of the measured oscillations of ΔT.

Phonon mode labeling	f_1	f_2	f_3	f_4
Bulk $CsPbCl_3$:				
Phonon frequency at 10 K (cm^{-1})[a]	36	55	76	95
Phenomenological parameter β (10^5 cm s^{-1})[b]	1.4	—	1.1	1.1
Nanocrystals of $CsPbCl_3$:				
Intrinsic phonon frequency f_0 (cm^{-1})	33.4	52.5	75.8	95.8
Anharmonic constant C (cm^{-1})	−0.7	−0.6	−1.6	−3.1
Temperature-independent phonon linewidth Γ_0 (cm^{-1})	1.3	—	0.3	<0.1
Anharmonic constant A (cm^{-1})	0.5	—	1.6	1.4

[a]Reference 21.

[b]Determined from Ref. 19 by fitting the calculated phonon-dispersion curves in the direction $\Gamma-M$.

values: $f_1=32.2$ cm^{-1}, $f_2=51.6$ cm^{-1}, $f_3=73.7$ cm^{-1}, and $f_4=92.3$ cm^{-1}.[23] These frequencies can be matched to the bulk $CsPbCl_3$ optical-phonon mode frequencies (see Table I). Because of the nanocrystalline morphology of $CsPbCl_3$, the presence of the confined and surface phonon modes is expected.[6–11] The standard Raman measurements in quasispherical NCs imply that the most important contribution comes from the confined phonon modes with $l=0$ (l is the orbital quantum number) and $n=1$.[9–11] For spherical NCs the frequencies ω^n of phonon modes with $l=0$ can be computed using[6]

$$(\omega^n)^2 = (\omega^{\text{bulk}})^2 - \beta^2\left(\frac{\nu_n}{R}\right)^2, \tag{1}$$

where ω^{bulk} is the bulk phonon frequency ($\omega=2\pi f$), β is a phenomenological parameter describing the phonon dispersion relation $\omega^2=\omega_0^2-\beta^2q^2$ (q is the phonon wavevector),[6] R is the NCs radius, and ν_n is the nth root of the spherical Bessel function j_1. The observed redshift of the frequencies of coherent oscillations in respect to the bulk phonon frequencies can be thus interpreted in terms of the phonon confinement. Indeed, the values of this frequency difference is in a rough agreement with the values of ($f^{\text{bulk}}-f^1$) predicted by Eq. (1) for $R=2$ nm, $n=1$, and the value of parameter β (given in Table I): 2.3 cm^{-1}, 0.7 cm^{-1}, 0.8 cm^{-1} for phonon modes 36 cm^{-1}, 76 cm^{-1}, and 95 cm^{-1}, respectively (the dispersion of phonon mode 55 cm^{-1} is not available in literature). The observed values of the frequency shifts are, in fact, slightly larger, which is probably caused by the deviation of NCs from the ideal spherical shape and/or by the contribution of phonon modes with $n>1$.

The experimentally measured oscillations can be decomposed into a sum of four exponentially damped sine-harmonic oscillations [see Eq. (1) in Ref. 23]. In Fig. 2(a), we show the measured oscillations of ΔT at 10 K (points) and the corresponding fit (solid line). The contributions of individual phonon modes to oscillations of ΔT are shown in Fig. 2(c) (solid curves). In our analysis, we assumed that the initial phase φ_0 is the same for all the phonon modes as expected for simultaneously excited independent oscillations. This assumption is validated by a very good quality of the fit [see Fig. 2(a)]. The observed identical initial phase for all phonon modes indicates an absence of the coupling between the phonon modes (cf. Ref. 13, where, unlike here, different values of the initial phase were reported for different phonon modes in $CdTe_{1-x}Se_x$ NCs). A weak intermode coupling in $CsPbCl_3$ can be expected because various phonon modes have their origins in different sublattice (ions) vibrations[19,29] [see, e.g., Fig. 1 in Ref. 19: phonon mode f_1…Cl ion vibration; f_3…Pb-Cl vibration; f_4…Cs, Pb, Cl vibration].

The mechanism of the coherent phonon dephasing can be identified by its temperature dependence.[30–32] When the temperature of semiconductor is increased, a decrease of the phonon frequency and an increase of the phonon relaxation rate due to anharmonic effects in the vibrational potential energy are usually observed.[30,31] Both the frequency shift and the damping constant are closely related; they correspond to the real and imaginary parts of the phonon self energy, respectively.[30] In general, an optical phonon can decay into two phonons (three-phonon process), three phonons (four-phonon process), or more phonons. In these processes, the energy and momentum conservation are obeyed. The probability of high-order processes rapidly decreases with lowering the temperature. Below the Debye temperature of a semiconductor, the three-phonon process is usually dominant.[33] In this case, the initial phonon with frequency f is split into two lower-energy phonons such that $f=f_a+f_b$. This can be realized either for $f_a=f_b$ (overtone channel) or $f_a\neq f_b$ (combination channel). The relative importance of overtone and combination channels depends on phonon-dispersion curves in particular material.[30–32] For the dominant role of the overtone channel, the temperature-induced shift of the phonon frequency f and the broadening of the phonon linewidth Γ (FWHM) resulting from the cubic anharmonicity are given by the expressions[30,33]

$$f(T) = f_0 + C[1 + 2n(f_a)] \tag{2}$$

and

$$\Gamma(T) = \Gamma_0 + A[1 + 2n(f_a)], \tag{3}$$

where T is the sample temperature, f_0 is the intrinsic frequency of the optical phonon, $n(f_a)=(e^{hf_a/kT}-1)^{-1}$ is the sta-

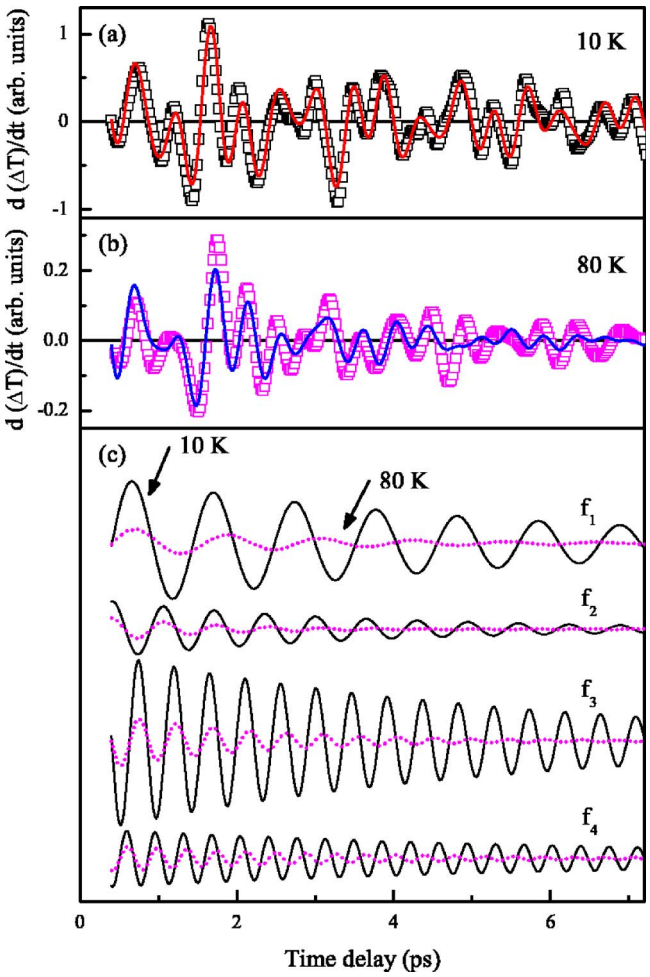

FIG. 2. (Color online) Time derivative of transmission change ΔT vs time delay between pump and probe pulses measured at 10 K (a) and 80 K (b) (points). The solid lines are fits by a sum of four exponentially damped sine harmonic oscillations.[34] Contributions of individual phonon modes to oscillations at 10 K (solid line) and 80 K (dotted line) are compared in (c).

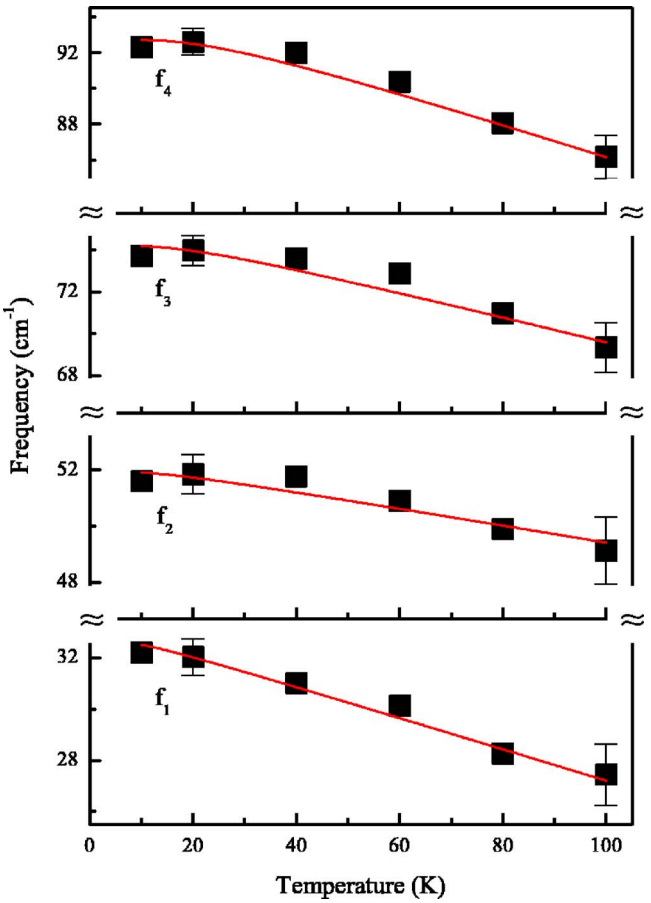

FIG. 3. (Color online) Temperature dependence of the frequency of phonon modes f_1, f_2, f_3, and f_4 determined by fitting a sum of four exponentially damped sine-harmonic oscillations to the experimentally measured oscillations of ΔT at various temperatures (points). The solid lines are fits by Eq. (2) with parameters given in Table I.

tistical occupation number of the phonon with frequency f_a ($f_a = f/2$), A and C are the anharmonic constants, and Γ_0 is the temperature-independent phonon linewidth.

When the sample temperature is increased, the oscillations observed in the measured signal of ΔT are less visible because of the decrease in both the phonon-mode amplitude and the dephasing time [see Fig. 1(b)]. As described above, the wavelength of the femtosecond laser pulses was tuned to follow the energy shift of the absorption spectrum during the measurements of the temperature dependence [laser pulse was centered at the spectral position corresponding to 418 nm at 10 K, as depicted by arrows in Fig. 1(a)]. With this condition obeyed, no systematic dependence of the phonon phase on the sample temperature was observed. In Fig. 2(b), we show the measured oscillations of ΔT at 80 K (points) and the corresponding fit (solid line). In Fig. 2(c), we compare the contributions of individual phonon modes to the measured oscillations of ΔT at 10 K (solid curves) with those at 80 K (dotted curves). The decrease in the phonon amplitude, the phonon frequency, and the oscillation damping time with the rising sample temperature is clearly apparent. The frequencies of the phonon modes in dependence on temperature are shown in Fig. 3 (points). When the temperature is increased, the phonon modes soften, in agreement with the data reported for bulk $CsPbCl_3$.[21] The solid lines in Fig. 3 are the fits using Eq. (2) with parameters given in Table I. The obtained values of anharmonic constant C are similar to those reported for other semiconductors.[30,31,33] The good agreement between the experimental data and the fits for all four phonon modes indicates that the temperature-induced shift of the optical-phonon frequency is dominated by the cubic overtone channel (decay of optical phonon into two isoenergetic acoustic phonons).

The measured temperature dependence of the phonon damping time τ is directly related to the broadening of the phonon linewidth Γ described by Eq. (3). Assuming the Lorenzian phonon line shape, the values of Γ can be determined from the simple formula $\Gamma = 1/(\pi c \tau)$, where c is the speed of light.[31] In Fig. 4, we show the temperature dependence of Γ, as derived from the measured values of damping time τ (points), and the fit using Eq. (3) (solid line) for three phonon modes (we do not have reliable data for phonon mode 52 cm^{-1} due to its low amplitude and fast damping).

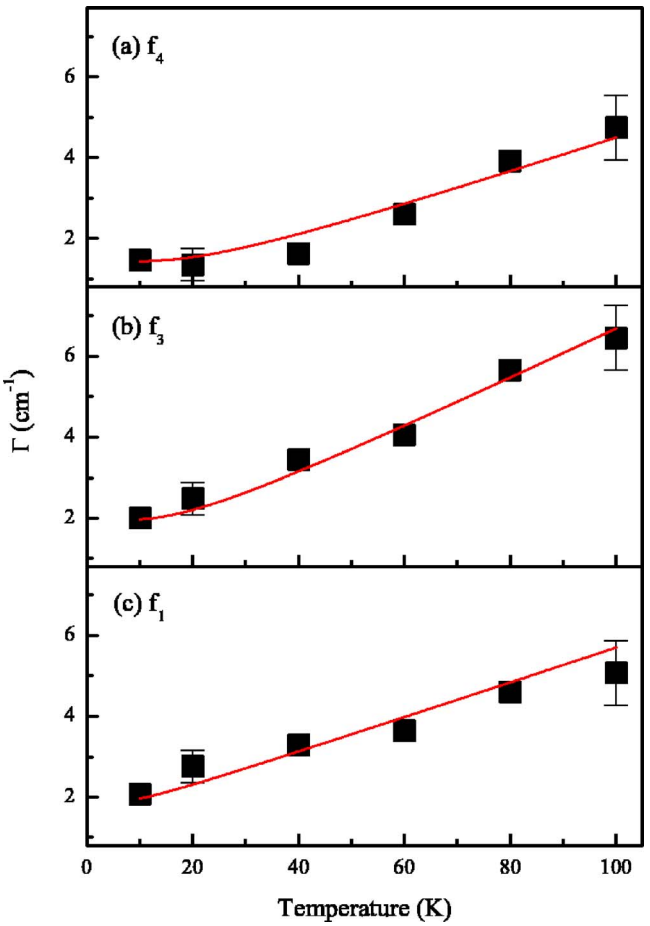

FIG. 4. (Color online) Temperature dependence of the phonon linewidth Γ of phonon modes f_1, f_3, and f_4 determined by fitting a sum of four exponentially damped sine harmonic oscillations to the experimentally measured oscillations of ΔT at various temperatures (points). The solid lines are fits by Eq. (3) with parameters given in Table I.

The obtained values of parameters Γ_0 and A are given in Table I. The values of anharmonic constant A are similar to those reported for other semiconductors.[30,31,33] The interesting fact is that the values of Γ_0 are rather small for phonon modes f_3 and f_4, whereas Γ_0 exceeds the value of A for phonon mode f_1. In bulk semiconductors, the temperature-independent phonon linewidth Γ_0 is usually explained as a consequence of an elastic scattering of coherent phonons by perturbing potential of lattice defects.[35] Consequently, the small value of Γ_0 for phonon modes f_3 and f_4 is a signature of a low concentration of defects in the sample investigated (including NC surface imperfections).[35] If the value of Γ_0 is negligible (like in the case of phonon mode f_4), the measured low-temperature relaxation rate fixes the only free parameter A in Eq. (3) (the occupation numbers are negligible for the temperature of 10 K). The good quality of the fit for phonon modes f_3 and f_4 confirms that their dephasing is dominated by the cubic overtone channel. The rather large value of Γ_0 for phonon mode f_1 indicates that another (temperature-independent) mechanism is also present. The temperature independence excludes the possible explanations based on additional phonon relaxation channels[32] (e.g., cubic combination channel, four-phonon processes, or phonon up-conversion) and/or interaction with other phonon modes (including the quantized bulk and/or surface phonon modes) because all these processes are proportional to the temperature-dependent occupation numbers.[32]

On the other hand, the temperature-independent phonon linewidth can be explained by two effects related to the spatial confinement of a phonon mode within NCs. First, the dispersion in the size distribution of NCs in the sample leads to a spread of phonon frequencies $\Delta f^{\text{distrib}}$ [see Eq. (1)]. Second, the bulk plane-wave-like phonon wave function cannot exist within small NCs, where the phonon cannot penetrate significantly beyond NCs surface into the surrounding matrix. The confined phonon is therefore composed of a "sum" of bulklike phonons. The phonon most similar to the bulk-zone center phonon, which participates in the optical experiments, possesses a range of wave vectors around the zone center. The spatial confinement leads to an "uncertainty" in the phonon wave vector Δq, $\Delta q \sim \pi/R$, where R is the NCs radius. Because of the $f=f(q)$ dependence this leads to a frequency uncertainty Δf^{conf}. The size-distribution-induced frequency spread $\Delta f^{\text{distrib}}$ is a property of an ensemble of NCs, while the confinement-induced frequency uncertainty Δf^{conf} is a property of the single NC. Nevertheless, both mechanisms are similar in their dependence on the dispersion of phonon modes. The considerably stronger dispersion of phonon mode f_1 than that of phonon modes f_3 and f_4 (see Fig. 2 in Ref. 19 and the values of β in Table I) leads to significantly larger frequency broadening for this phonon mode that is in accord with the experimental observations (see Table I). For the NCs radius $R=2$ nm (which leads to the wave-vector uncertainty $\Delta q \sim 1.5\times 10^7$ cm^{-1}) and the size distribution of 15%, the resulting upper estimates of the values of $\Delta f^{\text{distrib}}$ and Δf^{conf} for phonons with $n=1$ are (fortuitously) the same, namely, 1.9, 0.5, and 0.4 cm^{-1} for phonon modes f_1, f_3, and f_4, respectively. The comparison of these upper estimates of the line broadening with the values of Γ_0 given in Table I suggests that both effects may be responsible for the observed temperature-independent contribution to the linewidth.

To sum up, the measured temperature dependence of coherent phonon mode softening and dephasing in $CsPbCl_3$ NCs can be interpreted in terms of a mechanism typical of bulk semiconductors, namely, the cubic anharmonicity of the lattice. The nanocrystalline morphology of the sample leads only to minor modification of the process.

IV. CONCLUSION

Four different coherent optical-phonon modes were generated in $CsPbCl_3$ nanocrystals by femtosecond laser-pulse illumination. The observed phonon modes were matched to the bulk $CsPbCl_3$ optical-phonon mode frequencies, and the measured low-frequency shift was attributed to the phonon confinement in nanocrystals. A dominant contribution of phonon modes with $l=0$ and $n=1$ to the measured transmission oscillations and their negligible mutual coupling was identified. The obtained temperature dependence of the phonon mode softening and oscillation damping were interpreted

in terms of the effect of cubic anharmonicity of the lattice. The origin of the observed temperature-independent contribution to the phonon linewidth was discussed, and the nanocrystal-size distribution-induced frequency spread and/or confinement-induced frequency uncertainty were proposed as the responsible mechanisms.

The observation of a simultaneous generation of four coherent optical-phonon modes in this material can extend the potential applications of coherent phonons. Namely, the construction of a polychromatic source of coherent phonons at THz frequencies can be foreseen.

ACKNOWLEDGMENTS

The authors thank M. Nikl and K. Nitsch from the Institute of Physics of The Academy of Sciences of the Czech Republic for providing the samples and for valuable discussions. This work is a part of the research plan MSM 0021620834 that is financed by the Ministry of Education of the Czech Republic, and partly was supported by the Research Project No. IAA1010316 of the Grant Agency of the Academy of Sciences of the Czech Republic.

[1] R. Merlin, Solid State Commun. **102**, 207 (1997).
[2] W. A. Kutt, W. Albrecht, and H. Kurz, IEEE J. Quantum Electron. **28**, 2434 (1992).
[3] M. Hase, K. Mizoguchi, H. Harima, S. I. Nakashima, and K. Sakai, Phys. Rev. B **58**, 5448 (1998).
[4] T. E. Stevens, J. Kuhl, and R. Merlin, Phys. Rev. B **65**, 144304 (2002).
[5] U. Woggon, *Optical Properties of Semiconductor Quantum Dots*, Springer Tracts in Modern Physics Vol. 136 (Springer, Berlin, 1997).
[6] E. Roca, C. Trallero-Giner, and M. Cardona, Phys. Rev. B **49**, 13704 (1994).
[7] F. Comas, C. Trallero-Giner, N. Studart, and G. E. Marques, Phys. Rev. B **65**, 073303 (2002).
[8] A. V. Gommonnai, Yu. M. Azhniuk, V. O. Yukhymchuk, M. Kranjcec, and V. V. Lopushansky, Phys. Status Solidi B **239**, 490 (2003).
[9] Y. N. Hwang, S. Shin, H. L. Park, S. H. Park, U. Kim, H. S. Jeong, E. J. Shin, and D. Kim, Phys. Rev. B **54**, 15120 (1996).
[10] M. I. Vasilevskiy, A. G. Rolo, and M. J. M. Gomes, Solid State Commun. **104**, 381 (1997).
[11] R. Kostric and N. Romcevic, Phys. Status Solidi C **1**, 2646 (2004).
[12] R. W. Schoenlein, D. M. Mittleman, J. J. Shiang, A. P. Alivisatos, and C. V. Shank, Phys. Rev. Lett. **70**, 1014 (1993).
[13] A. V. Bragas, C. Aku-Leh, S. Costantino, A. Ingale, J. Zhao, and R. Merlin, Phys. Rev. B **69**, 205306 (2004).
[14] J. L. Machol, F. W. Wise, R. C. Patel, and D. B. Tanner, Phys. Rev. B **48**, R2819 (1993).
[15] U. Banin, G. Cerullo, A. A. Guzelian, C. J. Bardeen, A. P. Alivisatos, and C. V. Shank, Phys. Rev. B **55**, 7059 (1997).
[16] D. Frohlich, K. Heindrich, H. Kunzel, G. Trendel, and J. Treusch, J. Lumin. **18/19**, 385 (1979).
[17] I. P. Pashuk, N. S. Pidzyrailo, and M. G. Macko, Sov. Phys. Solid State **23**, 1263 (1981).
[18] P. Lecoq, M. Schussler, and M. Schneegans, Nucl. Instrum. Methods Phys. Res. A **315**, 337 (1992).
[19] M. M. Sinha and K. Wakamura, J. Phys. Chem. Solids **63**, 541 (2002).
[20] D. M. Calistru, L. Mihut, S. Lefrant, and I. Baltog, J. Appl. Phys. **82**, 5391 (1997).
[21] C. Carabatos-Nedelec, M. Oussaid, and K. Nitsch, J. Raman Spectrosc. **34**, 388 (2003).
[22] M. Nikl, K. Nitsch, K. Polak, G. P. Pazzi, P. Fabeni, D. S. Citrin, and M. Gurioli, Phys. Rev. B **51**, 5192 (1995).
[23] P. Němec, K. Nitsch, M. Nikl, and P. Malý, Phys. Status Solidi C **1**, 2670 (2004).
[24] A. Voloshinovskii, S. Myagkota, A. Gloskovskii, and S. Zazubovich, Phys. Status Solidi B **225**, 257 (2001).
[25] S. Kondo, K. Suzuki, T. Saito, H. Asada, and H. Nakagawa, J. Cryst. Growth **282**, 94 (2005).
[26] P. Němec, P. Malý, M. Nikl, and K. Nitsch, Appl. Phys. Lett. **76**, 2850 (2000).
[27] The exciton mass m was deduced from the reduced exciton mass $\mu=0.65m_0$ (Ref. 17) on the assumption of the equal effective masses of electrons and holes (Ref. 16).
[28] P. Němec, K. Nitsch, M. Nikl, and P. Malý (to be published).
[29] G. L. Hua, J. Phys.: Condens. Matter **3**, 1371 (1991).
[30] M. Balkanski, R. F. Wallis, and E. Haro, Phys. Rev. B **28**, 1928 (1983).
[31] P. Verma, S. C. Abbi, and K. P. Jain, Phys. Rev. B **51**, 16660 (1995).
[32] F. Vallee, Phys. Rev. B **49**, 2460 (1994).
[33] S. Anand, P. Verma, K. P. Jain, and S. C. Abbi, Physica B **226**, 331 (1996).
[34] The experimentally obtained data were fitted by Eq. (1) in Ref. 23 with the following parameters: (a) 10 K: $A_1=-0.49$, $f_1=32.2$ cm^{-1}, $\tau_1=5.1$ ps; $A_2=-0.22$, $f_2=51.6$ cm^{-1}, $\tau_2=3.3$ ps; $A_3=-0.65$, $f_3=73.7$ cm^{-1}, $\tau_3=5.3$ ps; $A_4=-0.21$, $f_4=92.3$ cm^{-1}, $\tau_4=7.2$ ps; and $\varphi_0=38.9°$. (b) 80 K: $A_1=-0.13$, $f_1=28.3$ cm^{-1}, $\tau_1=2.3$ ps; $A_2=-0.11$, $f_2=49.9$ cm^{-1}, $\tau_2=1.3$ ps; $A_3=-0.23$, $f_3=71.0$ cm^{-1}, $\tau_3=1.9$ ps; $A_4=-0.10$, $f_4=88.1$ cm^{-1}, $\tau_4=2.7$ ps; and $\varphi_0=54.1°$.
[35] M. Hase, K. Ishioka, M. Kitajima, K. Ushida, and S. Hishita, Appl. Phys. Lett. **76**, 1258 (2000).